Radiative forcing due to enhancements in tropospheric ozone and carbonaceous aerosols caused by Asian fires during spring 2008

Murali Natarajan,[1] R. Bradley Pierce,[2] Todd K. Schaack,[3] Allen J. Lenzen,[3] Jassim A. Al-Saadi,[1] Amber J. Soja,[4] Thomas P. Charlock,[1] Fred G. Rose,[5] David M. Winker,[1] and John R. Worden[6]

Received 22 July 2011; revised 24 January 2012; accepted 30 January 2012; published 27 March 2012.

[1] Simulations of tropospheric ozone and carbonaceous aerosol distributions, conducted with the Real-time Air Quality Modeling System (RAQMS), are used to study the effects of major outbreaks of fires that occurred in three regions of Asia, namely Thailand, Kazakhstan, and Siberia, during spring 2008. RAQMS is a global scale meteorological and chemical modeling system. Results from these simulations, averaged over April 2008, indicate that tropospheric ozone column increases by more than 10 Dobson units (DU) near the Thailand region, and by lesser amounts in the other regions due to the fires. Widespread increases in the optical depths of organic and black carbon aerosols are also noted. We have used an off-line radiative transfer model to evaluate the direct radiative forcing due to the fire-induced changes in atmospheric composition. For clear sky, the monthly averaged radiative forcing at the top of the atmosphere (TOA) is mostly negative with peak values less than -12 W/m^2 occurring near the fire regions. The negative forcing represents the increased outgoing shortwave radiation caused by scattering due to carbonaceous aerosols. At high latitudes, the radiative forcing is positive due to the presence of absorbing aerosols over regions of high surface albedo. Regions of positive forcing at TOA are more pronounced under total sky conditions. The monthly averaged radiative forcing at the surface is mostly negative, and peak values of less than -30 W/m^2 occur near the fire regions. Persistently large negative forcing at the surface could alter the surface energy budget and potentially weaken the hydrological cycle.

Citation: Natarajan, M., R. B. Pierce, T. K. Schaack, A. J. Lenzen, J. A. Al-Saadi, A. J. Soja, T. P. Charlock, F. G. Rose, D. M. Winker, and J. R. Worden (2012), Radiative forcing due to enhancements in tropospheric ozone and carbonaceous aerosols caused by Asian fires during spring 2008, *J. Geophys. Res.*, *117*, D06307, doi:10.1029/2011JD016584.

1. Introduction

[2] Tropospheric ozone and carbonaceous aerosols are known forcing agents that affect the radiative balance of the Earth-atmosphere system [*Forster et al.*, 2007] in addition to impacting the air quality. Their variability can change the net radiative flux at TOA and at the surface of the earth on a short time scale. Biomass burning (BB) is one of the important drivers causing this variability. BB includes fires initiated for the purpose of clearing vegetation and changing land-use as well as uncontrolled wildfires. A major portion of BB is attributable to anthropogenic activities. Emissions from BB include nitrogen oxides (NO_x), carbon monoxide, and non-methane volatile organic compounds that contribute to the formation of tropospheric ozone. BB is also a significant source of carbonaceous aerosols; globally, about 76% of the organic carbon (OC) and about 42% of the black carbon (BC) aerosols originate from BB. [*Bond et al.*, 2004].

[3] Greenhouse gases (GHG) including CO_2 and CH_4 have long lifetimes and they are well mixed in the atmosphere. As a result, they have long-term influences on global climate. In contrast, both ozone and carbonaceous aerosols have relatively short lifetimes in the troposphere. They are removed from the atmosphere over timescales of the order of days or weeks through wet and/or dry scavenging processes, and also, in the case of ozone, through chemical reactions. This short lifetime, combined with the inherent variability of the sources, results in spatial and temporal inhomogeneity in their distribution and radiative forcing. For example, local hot spots near fire zones may experience large increases in aerosol optical depth, and photochemistry along the fire plumes can lead to enhanced production of tropospheric ozone far away from the fires. During such fire events, the radiative impact on a regional scale could be quite significant even though, when averaged over the globe, the effect may be small. Increases in tropospheric ozone and absorbing aerosols like BC have a positive radiative forcing while the

[1] NASA Langley Research Center, Hampton, Virginia, USA.
[2] NOAA/NESDIS/STAR, Madison, Wisconsin, USA.
[3] SSEC, University of Wisconsin, Madison, Wisconsin, USA.
[4] National Institute of Aerospace, Hampton, Virginia, USA.
[5] Science Systems and Applications, Incorporated, Hampton, Virginia, USA.
[6] Jet Propulsion Laboratory, Pasadena, California, USA.

0148-0227/12/2011JD016584

increases in scattering aerosols have a negative forcing at TOA. The potential for such short-term influences on regional scale radiative forcing has led to the suggestion that decreases in the emissions of absorbing aerosols could possibly alleviate the effect of global warming temporarily [*Jacobson*, 2002; *Bond and Sun*, 2005; *Ramanathan and Carmichael*, 2008]. On the other hand, the presence of scattering aerosols helps to mitigate the effects of positive forcing due to long-lived GHG. Increases in anthropogenic aerosols can also alter the surface energy budget and lead to a weakening of the hydrological cycle through a reduction in evaporation [*Ramanathan et al.*, 2001; *Liepert et al.*, 2004]. Estimates of radiative forcing caused by changes in the atmospheric abundance of these drivers generated by BB are of interest, especially if control measures on anthropogenically initiated BB activities are to be considered in the future. The aim of the present work is to evaluate the radiative impact of the changes in tropospheric ozone and OC and BC aerosols triggered by the Asian fire events that occurred during the spring of 2008.

[4] Radiative effects of tropospheric ozone have been studied in the past through combinations of global scale models and observations. Estimates of the radiative forcing due to increases in tropospheric ozone, caused by all anthropogenic emissions of NOx, CO, and non-methane hydrocarbons, relative to pre-industrial times are given by *Gauss et al.* [2006]. These results are taken from various chemical transport models (CTM) and coupled chemistry-climate models. Globally and annually averaged change in tropospheric ozone column since pre-industrial times ranges from 7.9 to 13.8 DU. The corresponding direct radiative forcing (DRF) averaged over the models is 0.32 W/m^2. The present work, in contrast, focuses on only one source of perturbation to tropospheric ozone, namely BB emissions, and that too over a limited period of time. *Joiner et al.* [2009] make use of tropospheric ozone column derived from the Ozone Monitoring Instrument (OMI) and the Microwave Limb Sounder (MLS) experiments aboard the Aura satellite to calculate the radiative effect of tropospheric ozone. Their baseline case considers no tropospheric ozone and hence the calculated forcing represents an upper bound for the RF given by *Forster et al.* [2007]. *Naik et al.* [2005] used the MOZART-2 model to evaluate the changes in tropospheric ozone due to a 10% reduction in the anthropogenic emissions in 9 different regions, and calculated the radiative forcing using the Geophysical Fluid Dynamics Laboratory (GFDL) radiative transfer model. They highlight the sensitivity of the ozone change and radiative forcing to season and geographical location of the perturbations in emissions. They also note that the radiative forcing is larger when the emissions of all the ozone precursors are reduced simultaneously. The present study also uses a global scale model to evaluate the changes in tropospheric composition, but the perturbation in BB emission, which is the driving force, is not a fixed amount and it varies both in time and with location.

[5] Calculated distributions of BC and OC aerosols are used in this study in conjunction with specified optical properties to evaluate the radiative impact of BB aerosol emissions. We use satellite data in deriving the BB emissions of various species. Some of the earlier studies have used optical properties derived from measurements to calculate the DRF of aerosols [*Hobbs et al.*, 1997, *Ross and Hobbs*, 1998]. DRF from smoke aerosols generated by the Brazilian fires changes from -26 ± 6 W/m^2 over a dark surface such as ocean to 25 ± 12 W/m^2 over a reflective surface such as a desert [*Ross and Hobbs*, 1998]. In a case study of the solar radiative forcing by BB aerosols during SAFARI 2000 campaign, *Keil and Haywood* [2003] report the change of DRF at TOA from negative (cooling) to positive (warming) due to the presence of underlying cloud. *Hsu et al.* [2003] use satellite data to investigate the impact of smoke aerosols on reflected shortwave radiation from underlying cloud.

[6] Global scale models have been used in many studies to calculate the DRF of carbonaceous aerosols. For example, *Reddy et al.* [2005] use a General Circulation Model to estimate the relative impact of aerosols from fossil fuels, BB, and natural sources on globally and annually averaged AOD and DRF. *Naik et al.* [2007] report the DRF due to regional reduction in BB emissions, which include OC and BC aerosols in addition to tropospheric ozone precursors. They conclude that a reduction in BB emissions results in negative RF at TOA and that the impact depends on the geographical location of the emissions. *Chung et al.* [2005] use a different approach involving MODIS, AERONET, and GOCART aerosol products and ISCCP cloud data to develop anthropogenic aerosol distributions needed for radiative calculations. Their results show large regional differences in total surface forcing with tropical Asian regions displaying the largest contribution. They caution against heavy reliance on global mean forcing when assessing the role of aerosols. *Wang et al.* [2007] studied the regional climatic effects of BB emissions in Asia during the TRACE-P campaign time period. They consider a model domain spanning South and East Asia, and use the Hybrid Single-Particle Lagrangian Integrated Transport (HYSPLIT) model to calculate the distributions of OC and BC aerosols during March 2001. They use the CLIRAD-SW model developed by *Chou and Suarez* [1999] to evaluate the DRF. Unlike the present work, *Chung et al.* [2005] and *Wang et al.* [2007] do not consider the effects of tropospheric ozone changes.

[7] The main focus of this study is on the widespread fires that occurred in 3 major areas of Asia, namely Thailand, Kazakhstan, and Siberia over an extended period during the spring season in 2008. Figure 1 shows the three regions, labeled **A**, **B**, and **C**, in a composite of the locations of fires from April 10 to April 19, 2008, detected by the Moderate Resolution Imaging Spectroradiometer (MODIS) experiment (http://rapidfire.sci.gsfc.nasa.gov/firemaps/). The red color indicates low fire counts and the yellow color corresponds to high fire counts. The fires in the Kazakhstani region were primarily agricultural burning whereas those in the Lake Baikal region of Siberia were mostly secondary forest fires [*Warneke et al.*, 2009]. Most of the fires in the Thailand region were due to land clearing and/or agricultural burning. BB during spring is an annual occurrence in the Thailand (**A**) region. Early season burning is quite typical in Kazakhstan (**B**) and Siberia (**C**) [*Loboda and Csiszar*, 2007; *Soja et al.*, 2004], but during the spring of 2008 these regions experienced increased burning and many of these fire events burned out of control. These uncontrolled wildfires exhibited large day-to-day variability. The transport of the smoke plumes from these fires across the Pacific and into the Arctic region has been identified by satellite and aircraft observations and related analyses that were conducted during and after the

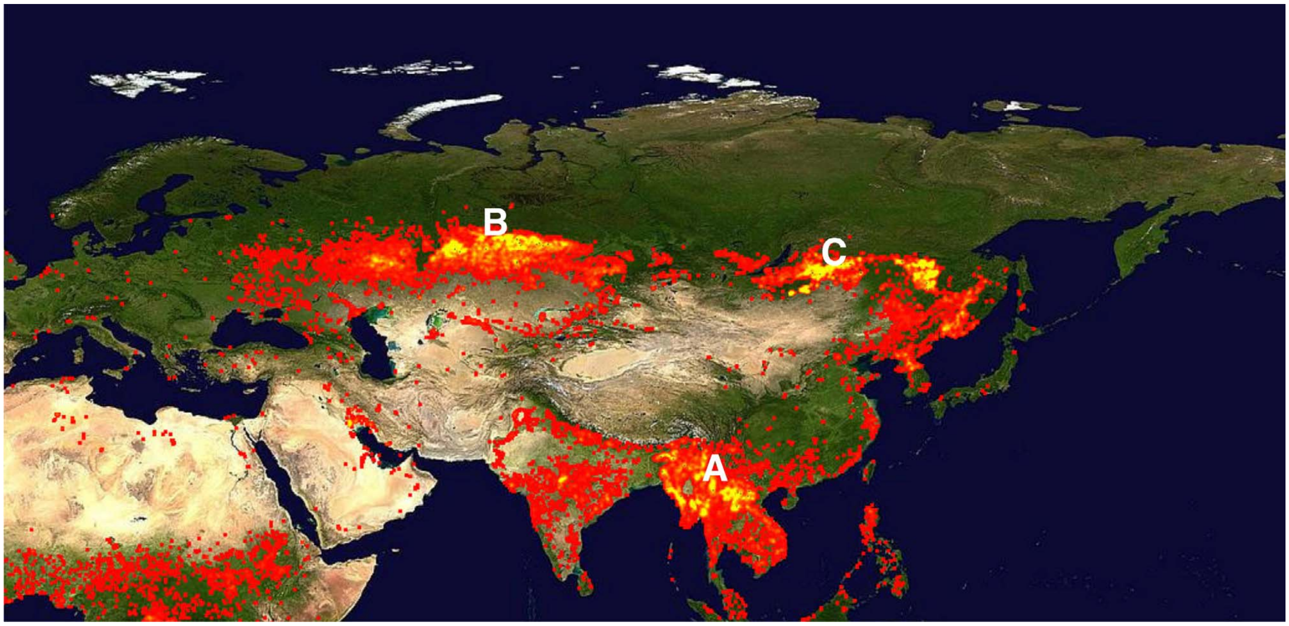

Figure 1. Map of fire locations for the period from April 10 to April 19, 2008, generated by the MODIS rapid response system, obtained from NASA/GSFC Rapid Response system (http://rapidfire.sci.gsfc.nasa.gov/firemaps/). Thailand (region **A**), Kazakhstan (region **B**), and Siberia (region **C**).

Arctic Research of the Composition of the Troposphere from Aircraft and Satellites (ARCTAS), and Aerosol, Radiation, and Cloud Processes affecting Arctic Climate (ARCPAC) campaigns [*Warneke et al.*, 2009, 2010; *Dupont et al.*, 2012]. We have used a 3-dimensional air quality model to simulate the atmospheric composition during the spring and summer of 2008 as a part of our support to the ARCTAS and ARCPAC campaigns. Additional sensitivity simulations conducted with and without the Asian fires are used in this study to evaluate the changes in tropospheric composition attributable to these fires. Radiative flux calculations, performed using an offline radiative transfer model, help us evaluate the direct radiative impact of the fires.

[8] A description of the air quality model including the input data related to the fire events is given in section 2. This is followed by a discussion of the calculated species distributions from the baseline model and the changes caused by the Asian fire. In section 3, we present a brief description of the radiative transfer model and a discussion of the RF results. Summary and conclusions make up the last section.

2. Atmospheric Composition

2.1. Model Description

[9] The main tool used for modeling the atmospheric chemical composition is the Real-time Air Quality Modeling System (RAQMS) developed jointly at the NASA Langley Research Center and the University of Wisconsin (LaRC/UW). The global scale meteorological and chemical modeling system has been used for assimilating remotely observed atmospheric chemical composition and forecasting the air quality within selected regions of the Earth [*Pierce et al.*, 2003, 2007]. The dynamical core for the global version of RAQMS is the UW hybrid isentropic coordinate model [*Schaack et al.*, 2004]. This model has previously been used to provide chemical forecasts to assist in flight planning during airborne campaigns such as INTEX-A and INTEX-B. The present study is somewhat similar to a post mission reanalysis except that some of the data assimilations are not included.

[10] The simulations are conducted on $2^\circ \times 2^\circ$ horizontal resolution. The vertical domain of the model extends from the surface to upper stratosphere. The model has 35 levels in the vertical, and uses isentropic coordinates in the stratosphere and a hybrid system in the troposphere. The top level of the model is 2600K and the pressure at the top ranges between 0.7 and 0.4 hPa. The model run begins on February 15, 2008 and the results from April 2008 are used for the analysis described in this study. The meteorological fields are initialized with the NOAA Global Forecasting System (GFS) analysis every 6 h. We include assimilation of stratospheric ozone profile data from the MLS instrument aboard the Aura satellite. Assimilations of total ozone from the OMI experiment, and of aerosol optical depth from the MODIS experiment, which were done in support of ARCTAS campaign-related studies, are turned off for the present study. This enables us to evaluate the changes in tropospheric ozone and OC and BC aerosols caused by the Asian fires.

[11] Photochemical mechanisms that control the formation and destruction of ozone in both stratosphere and troposphere are included through a unified module. A detailed description of the formulation is given by *Pierce et al.* [2007]. The photochemical reaction rate data recommended by *Sander et al.* [2003] are used. Current version of FAST-J2, a code to evaluate the photolysis rate constants [*Bian and Prather*, 2002], is used. The photolysis rate constants are dependent on the calculated ozone vertical profile, aerosol optical depth, and cloud parameters. RAQMS incorporates the Goddard Global Ozone Chemistry Aerosol Radiation and Transport (GOCART) model [*Chin et al.*, 2002] to evaluate and apply

Table 1. Regional and Global Surface Emissions of CO, BC, OC, and NO Integrated Over April 2008[a]

Region	CO_{bb}	CO_o	BC_{bb}	BC_o	OC_{bb}	OC_o	NO_{bb}	NO_o
A	32.4	13.4	0.33	0.08	2.67	0.17	0.4	0.28
B	17.0	1.96	0.17	0.007	1.36	0.008	0.26	0.12
C	11.3	0.22	0.10	0.0005	0.83	0.0007	0.15	0.01
Global	88.87	67.8	0.92	0.38	7.37	0.69	1.28	2.57

[a]Subscript 'bb' refers to biomass burning source and 'o' refers to the sum of other sources such as fossil fuel and soil emissions. Altitude dependent NOx source from lightning and aircraft emissions are included in the model but not in this table. The units are Tg of CO, Tg of C for BC and OC, and Tg of N.

the aerosol tendencies for settling, dry deposition, and chemistry. The input data for GOCART include OH concentration and horizontal wind that are calculated in the RAQMS model. Aerosol types considered in the model are sulfate, BC, OC, dust, and sea salt. Both hydrophilic and hydrophobic types of carbonaceous aerosols are included. We treat the aerosols as externally mixed. RAQMS formulation includes surface removal of species such as O_3, CO, nitric acid, peroxides, and aerosols by dry deposition. Soluble species are also removed by wet scavenging using a scheme based on convective fluxes and precipitation amounts [*Pierce et al.*, 2007].

[12] Surface emissions of NOx and CO, other than those from BB, are based on climatological databases [*Olivier et al.*, 1996]. Data for Asian emissions for the year 2000 have been adopted from *Streets et al.* [2003]. Emissions of NOx from lightning and aircraft are also included. Specification of BB emissions is of primary significance for the present study. These emissions invariably exhibit large spatial and temporal variability. To incorporate this variability adequately, RAQMS makes use of data from the MODIS instrument aboard Terra and Aqua satellites in constructing a database of daily emissions from BB. The location, timing, and the area covered by the burning are obtained from the MODIS Rapid Response Fire Detection data. An eco-system dependent carbon fuel consumption database is used to estimate the carbon emissions under low, medium, and high fire weather severity conditions. Meteorology-based estimate of the fire weather severity is made using the U.S. Forest Service Haines Index. The above data are combined to get the direct emission of carbon due to BB worldwide during spring and summer of 2008 [*Al-Saadi et al.*, 2008]. Separate estimates for day and night conditions are developed. Emission fluxes for CO, NO, C_2H_6, propane and higher parafins, ethene and higher olefins, HCN, CH_3CN, and carbonaceous aerosols are determined using known emission ratios relative to carbon. The emission ratio OC/BC is assumed to be 8, and 80% of BC and 50% of OC are treated as hydrophobic, following the assumptions used in GOCART. The present study does not consider the emission of sulfur compounds by BB. Smoke injection height is parameterized based on the vegetation type and fire weather severity. The injections occur mostly within the planetary boundary layer and this is in accordance with the findings of *Kahn et al.* [2008].

[13] A comparison of the emissions from BB with other surface sources for selected species is shown in Table 1. These are emissions integrated over the month of April 2008 and over the different regions **A** (80°E-120°E, 10°N-30°N), **B** (30°E-90°E, 50°N-60°N), **C** (110°E-140°E, 50°N-60°N), and the entire globe. Based on this model input data, BB represents a significant source of all these species especially in the regions under consideration. We have not shown the data for the volatile organic carbon, which are estimated using scaling factors with respect to carbon emissions, and the altitude dependent sources of NO due to lightning and aircraft emissions in this table. We recognize that model estimations of BB emissions could have large uncertainties. *Al-Saadi et al.* [2008] have compared the BB emissions in RAQMS for different periods in 2006 over contiguous United States domain with estimates from three other techniques, which also use satellite data to determine the area burned. They note that while there was consistency in temporal evolution and spatial pattern, monthly emission estimates differed by nearly an order of magnitude. They also compared the model predictions of CO with satellite data and found that in 3 out of 4 regions of large BB in the tropics, the RAQMS had a high bias.

2.2. Model Results and Evaluation

[14] Past studies, through comparisons with available observations, have demonstrated the capability of RAQMS to simulate the impact of boreal fire plumes [*Pierce et al.*, 2007; *Verma et al.*, 2009; *Dupont et al.*, 2012]. These studies made use of Tropospheric Emission Spectrometer (TES) observations of CO to identify the plumes. Backward and forward trajectories were used to confirm the origin of the plume, and through sampling of the RAQMS results for an ensemble of trajectories, the chemical evolution of the fire plume was examined. For the present study we employ the RAQMS model in a different manner. By conducting RAQMS simulations with and without the BB emissions from the three selected Asian regions, we generate baseline and perturbed model atmospheres so that the differences between them could be attributed to the Asian fires. We will first look at representative results from the baseline simulation (which includes the Asian fires) and comparisons with available observations.

2.2.1. Tropospheric Aerosols

[15] We have utilized the global scale observations of aerosols obtained by the Cloud-Aerosol Lidar with Orthogonal Polarization (CALIOP) instrument for comparisons with RAQMS model results. CALIOP, which is the main instrument aboard the Cloud-Aerosol Lidar Infrared Pathfinder Satellite Observations (CALIPSO) satellite, provides high-resolution vertical profiles and physical properties of clouds and aerosols [*Winker et al.*, 2007]. The satellite began its operations in 2006 as a part of the "A-Train" constellation. The observed total aerosol extinction, during the month of April 2008, is shown as a function of latitude and altitude in Figure 2 (left). We have used a log scale to display the large range of extinction values. Both day and night data obtained in the longitude sector from 90°E to 135°E have been used in generating this plot. Only data with a cloud-aerosol discrimination (CAD) score of less than −20 are considered, thereby assuring that the extinction values are predominantly due to aerosols. The high aerosol extinction seen in the 10°N to 50°N latitude range and at low altitudes is most likely due to the influence of Asian wildfires that occurred throughout the month in this region. The vertical extent of this perturbation reaches more than 5 km. Figure 2 (right) shows the monthly averaged total aerosol extinction from the RAQMS

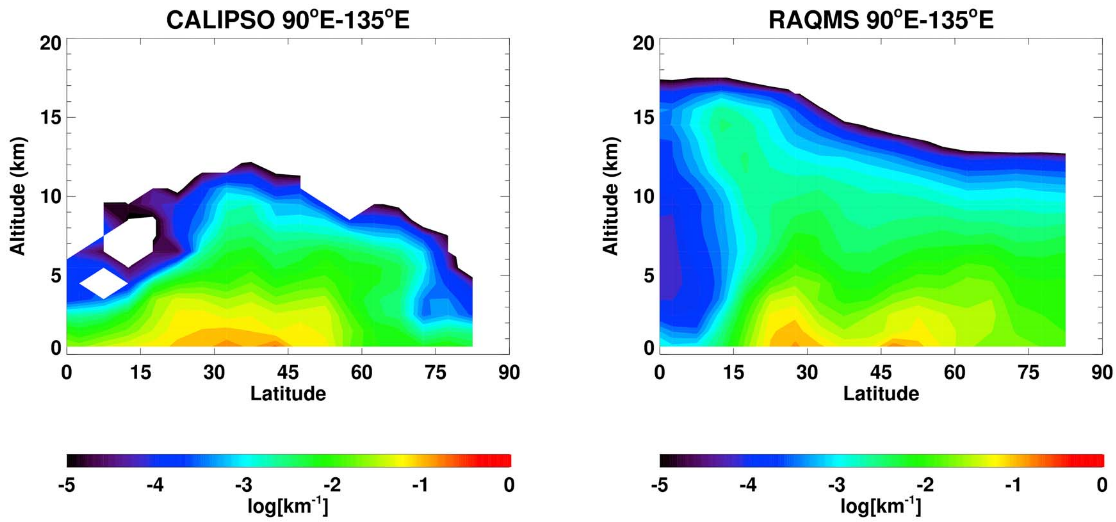

Figure 2. Total aerosol extinction at 532 nm (km^{-1}) in the longitude sector from 90°E to 135°E, and averaged over April 2008. (left) CALIPSO observations; (right) RAQMS extinction interpolated to CALIPSO locations and time.

baseline model for the same longitude sector. The model results have been interpolated to CALIOP measurement times and locations. The calculated extinction in the mid latitude lower troposphere agrees well with the CALIOP data but the RAQMS model seems to overestimate the extinction near the surface at high latitudes and also in the tropical upper troposphere. A comparison of our baseline and perturbed model results indicate that most of the extinction in the tropical upper troposphere is due to BB emissions from outside the boundaries of regions **A**, **B**, and **C**. An analysis of the latitudinal variation of the AOD averaged over 90°E to 135°E shows that more than 50% of the total AOD in the northern hemisphere during April 2008 is due to carbonaceous aerosols. In a study of aerosol distributions using CALIPSO and MODIS observations from June 2006 to November 2007 and results from GOCART model simulations, *Yu et al.* [2010] report discrepancies in the magnitude of AOD in many regions. They show that the CALIOP extinctions are smaller than the GOCART values near the surface and in the free troposphere for most of the seasons over eastern China. While these conclusions are qualitatively similar to our findings, the reasons for these model-data differences are presently unclear.

[16] As mentioned earlier, both air quality and radiative balance are affected by the enhancements in carbonaceous aerosols emitted by BB. The aerosol variations obtained in the RAQMS baseline simulation are illustrated in the form of time series plots in Figure 3 for two locations, Taihu (120.2°E, 31.4°N) and Barrow (156.7°W, 71.3°N). The top two panels show the calculated variations in total aerosol extinction as a function of time and altitude. Taihu is very close to the fire zone labeled **A** in this study and large extinction is seen both near the surface and above. In contrast, peak extinction at Barrow, which is far away from the fire zones, occurs in the 2 to 6 km altitude range. In both locations, the day-to-day fluctuation in extinction is quite noticeable. High extinction in the upper levels at both locations indicates lofting and transport effects on the fire plumes.

[17] Ground–based optical monitoring of aerosols has been conducted since 1993 as a part of the Aerosol Robotic Network supported by NASA and various governmental agencies throughout the world [*Holben et al.*, 1998]. Both Taihu and Barrow are AERONET sites and the 550 nm AOD measured at these sites during April 2008 are shown as red dots in Figure 3 (bottom). The time series of RAQMS AOD interpolated to these two locations are also shown in these panels. At Taihu, RAQMS values are lower than the measurements. The correlation coefficient is about 0.54 and the bias is −0.55. In the earlier section, we had noted that the RAQMS extinction in the Asian region was slightly high biased relative to CALIOP measurements. These comparisons show that RAQMS AOD falls in between the AERONET and CALIOP data in the Asian region. The RAQMS arctic AOD is in good agreement with the AERONET data as seen in the comparison at Barrow, shown in Figure 3 (bottom right). The correlation coefficient here is about 0.51 and the bias is only −0.07. For a global scale comparison, a scatterplot of the AERONET optical depth at 550 nm and the RAQMS optical depth is shown in Figure 4 (left). We use interpolation to get RAQMS AOD corresponding to the time and location of individual AERONET observations made during April 2008 at 167 locations around the world. The correlation coefficient is about 0.41 and the mean bias is −0.126 with RAQMS values lower than the AERONET data. In a study of atmospheric aerosol distribution from 2000 to 2007 using the GOCART model, *Chin et al.* [2009] report that the model underestimates the optical depth by 30–40% in the case of BB aerosols. The histogram of AOD at 550 nm given in Figure 4 (right) shows peak modes at lower values of AODs from RAQMS, which are not seen in the AERONET data. However, for AOD greater than 0.1, there is clear evidence of underestimation by the model, thus resulting in an overall negative bias.

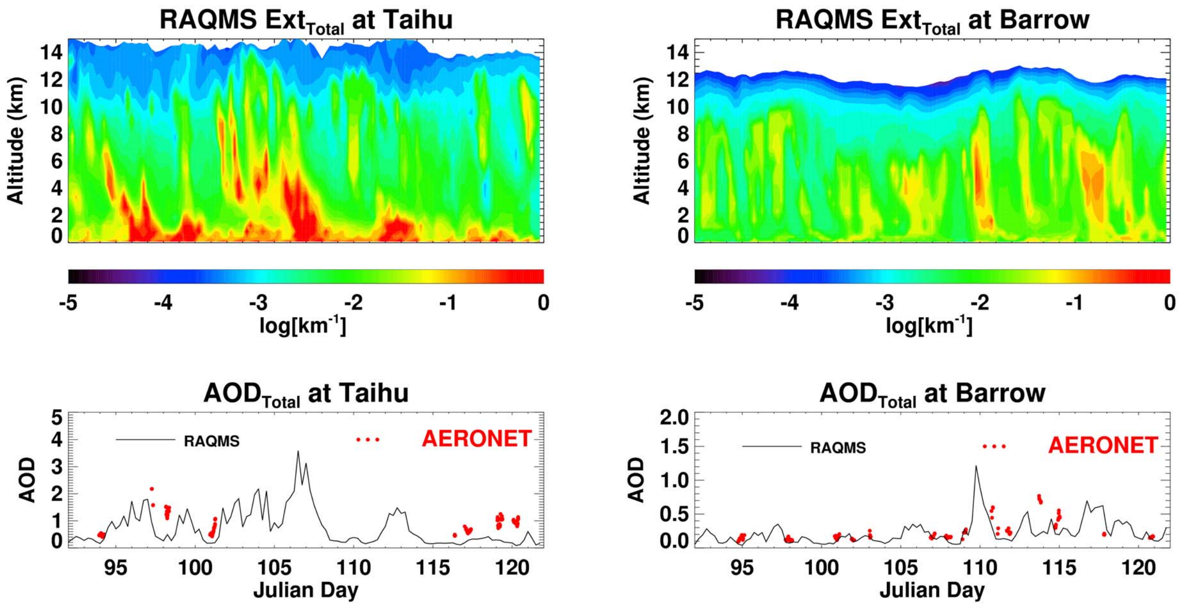

Figure 3. (top) Time series, during April 2008, of RAQMS total aerosol extinction. (left) at Taihu (120.2°E, 31.4°N); and (right) at Barrow (156.7°W, 71.3°N). (bottom) Time series of RAQMS total aerosol AOD (black line) and AERONET data (red dots) at 550 nm. (left) at Taihu (r = 0.55, bias = −0.54); and (right) at Barrow (r = 0.51, bias = −0.07).

2.2.2. Tropospheric Ozone

[18] We make use of the ozone measurements made by the Tropospheric Emission Spectrometer (TES) experiment for comparisons with the model derived ozone distributions in the troposphere during April 2008. The TES instrument was part of the payload aboard the Aura satellite launched in 2004. It is an infrared, Fourier transform spectrometer, which measures the thermal emission of the surface and the atmosphere. Vertical profiles of tropospheric ozone, CO, and various other trace gases are retrieved from this data on a global scale [*Beer et al.*, 2001]. Detailed description of the experiment and validation of the tropospheric ozone data are given by *Worden et al.* [2007]. For the present study, we focus on the data obtained during April 2008 in the longitudinal sector 90°E to 135°E and in the northern hemisphere. This longitudinal sector includes the fire zones of Thailand and Siberia. We first interpolate the RAQMS results to TES observation locations within the selected spatial domain and measurement time. Since the TES vertical resolution is coarser than the model vertical grid, we apply the TES averaging kernel (AK) to the ozone profiles from RAQMS. The resulting ozone distribution from the model averaged over the month is shown in Figure 5 (middle). Figure 5 (left) shows the corresponding ozone distribution from the TES observations. The model bias as a percent difference is shown in Figure 5 (right). The dark line at the top represents the average location of the model tropopause. Intrusion of stratospheric air mass is the major reason for mixing ratios higher than 150 ppbv indicated by yellow and red regions near the tropopause. The agreement between the two distributions is quite good except near the tropopause for latitudes greater than 35°N. The model ozone is generally within

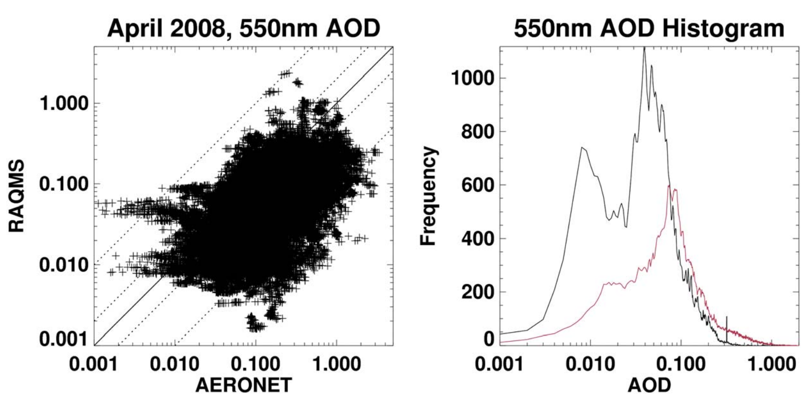

Figure 4. Comparison of aerosol optical depth (AOD) at 550 nm from RAQMS model and AERONET observations worldwide during April 2008. (left) Scatterplot for April 2008, r = 0.41, RMS = 0.22, Mean bias = −0.127; (right) Histogram of AOD from RAQMS (Black) and AERONET (Red).

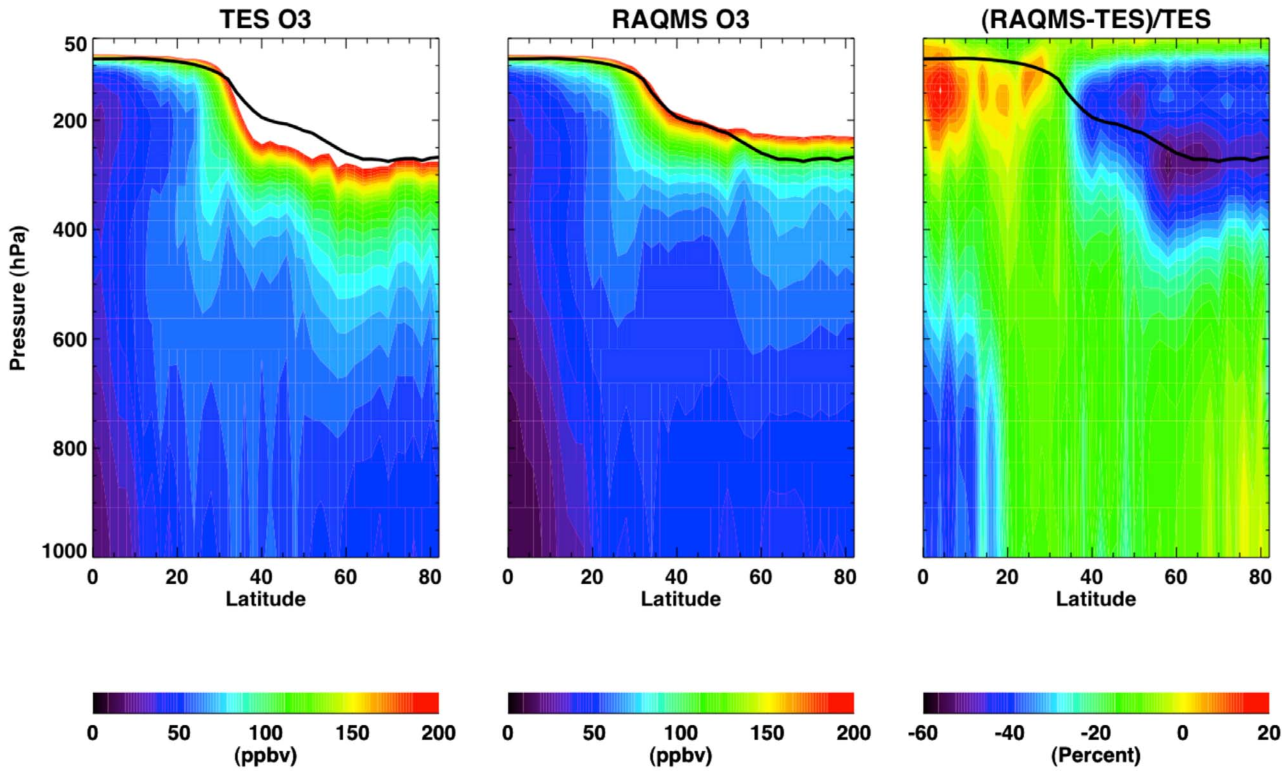

Figure 5. Tropospheric ozone mixing ratio (ppbv) in the longitude sector from 90°E to 135°E, and averaged over April 2008. (left) TES observations; (middle) RAQMS results interpolated to TES observation locations and time, and scaled with TES averaging kernel; (right) percent difference between RAQMS and TES.

+/−20% of the TES observations. Larger disagreements are seen near the tropopause at high latitudes, with RAQMS showing a low bias of nearly 50% compared to TES ozone. The high latitude differences near the tropopause are most likely due to an underestimation of the stratosphere-troposphere exchange in the RAQMS model. We note that for the present study we have included the assimilation of MLS ozone in the stratosphere (for pressures < 50 hPa). The model low bias occurs mostly in the 150 – 350 hPa region. In the mid to upper troposphere near the Thailand fire zone (25°N to 30°N), the calculated ozone is within 15% of the TES observations.

[19] A time series of tropospheric ozone at a selected location from the baseline model, which includes the Asian fires, is shown in Figure 6 (left). Figure 6 (right), which shows the difference in the time series between the model runs with and without the Asian fires, illustrates the impact of the fires during April 2008. The location chosen for this comparison corresponds to the ozonesonde station at Naha, Japan (127.7°E, 26.2°N). The vertical dashed lines denote the 4 days when ozonesonde measurements were made at Naha. Large increases in ozone mixing ratio resulting from the BB emissions are noted throughout the month. The ozone perturbations occur even in the upper troposphere as seen, for example, around Julian day 103 (April 12) near 250 hPa. Comparisons of the ozonesonde observations and the calculated profiles corresponding to the 4 days of observations are shown in Figure 7. The ozonesonde data were obtained from the World Ozone and Ultraviolet Radiation Data Center (WOUDC) in Toronto, Canada. The model values shown are at 6Z, which is within 30 min of the local time of measurements. The high mixing ratios near 100 hPa represent intrusions of stratospheric ozone. This is corroborated by Figure 6, which shows no significant difference at this level between the baseline and perturbed simulations. The observation on April 11 indicates a dramatic increase in the mixing ratio for the entire profile. Calculated O_3 profile also shows an increase but the mixing ratios are lower than the observations. However, as seen in the time series (Figure 6), the calculated O_3 around 250 hPa shows even larger increases on April 12. We have studied the ozone sensitivity to individual fires by turning off emissions one region at a time. The results (not shown) indicate that the variability in calculated tropospheric ozone at Naha is mostly due to the fires in Thailand region. The large impact on the free tropospheric ozone seen in the model results is an indication of the lofting of the fire emissions due to transport.

[20] The above comparisons demonstrate that the baseline RAQMS simulation, which includes emissions from all the BB, yields ozone and aerosol distributions which are in reasonable agreement with available data in the region of interest.

2.3. Impact of Asian Fires on Tropospheric Composition

[21] The calculated changes in tropospheric composition that are attributable to the Asian fires are discussed in this section. We will focus only on the changes in tropospheric

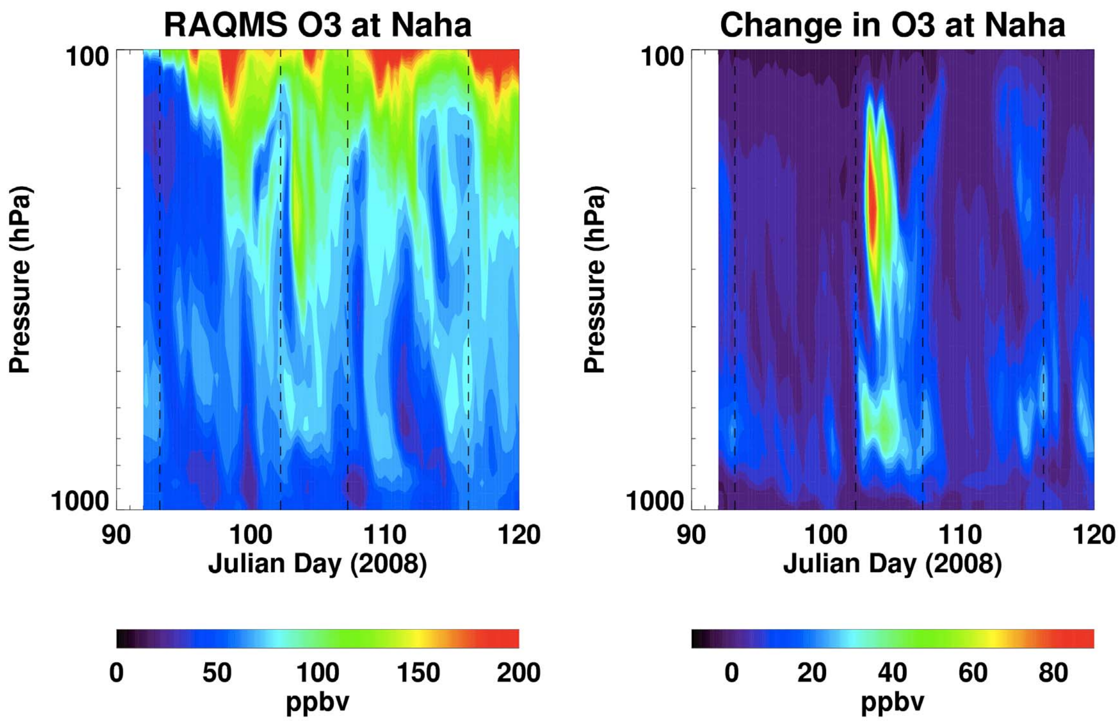

Figure 6. (left) Time series of ozone mixing ratio profile from baseline run (with Asian fires) of the RAQMS model interpolated to 127.7°E and 26.2°N (Naha) during April 2008; (right) Time series of the difference in ozone mixing ratio between the baseline (with Asian fires) and the perturbed (without Asian fires) model runs.

ozone and carbonaceous aerosols since they exert a major influence on the regional scale radiative balance. The results described here are the differences between the baseline simulation incorporating all the BB emissions and the perturbed case in which the emissions from the Asian fires (regions marked **A**, **B**, and **C** in Figure 1) are excluded. Emissions from BB, especially those from wildfires, are characterized by large variability over short time scales. This, combined with the changing atmospheric transport characteristics, results in daily variations in the distributions of tropospheric ozone and carbonaceous aerosols. We illustrate this variability by showing the results for two days, one during and the other following periods of high thermal anomalies seen in MODIS data. Around April 9 regions **A** and **B** experienced high fire counts, and region **C** had peak fire emissions around April 17. Later, we show monthly averaged results, which are more meaningful from the point of view of regional impact on air quality and radiative forcing.

[22] The change in tropospheric ozone integrated from the surface to the model tropopause for April 10 is shown in Figure 8 (left). The maximum value of about 24 DU occurs in the region **A** and values of the order of 10 DU are seen around this region extending into China. Large emissions of precursors like CO and NOx from the fire and the transport of the fire plume through regions known for high anthropogenic sources of pollution lead to enhanced production of ozone. The low latitude location is also conducive to more active photochemistry. In contrast, the high latitude fire regions of Kazakhstan and Siberia (near regions **B** and **C**) do not show any significant increase in tropospheric ozone column. Increases in ozone column, though small, are seen far away from the fire zone around the globe at 30N on April 10. This is most likely due to the fires that occurred in region **A** prior to April 1, because only these air masses would have had enough time to spread eastward across the Pacific and go even further in 10 days. Figure 8 (middle and right) shows the calculated changes in the BC and OC optical depths at 550 nm for April 10. The peak values of optical depths are collocated with the peak fire emissions in all the regions. The effect of transport is also noticeable in these maps. We note that this model considers all aerosols to be externally mixed. The optical properties and hence the optical depth could be different if internal mixing of two or more aerosols were allowed to occur. Calculated changes for April 22 are shown in Figure 9. Figure 9 (left) shows that the changes in tropospheric ozone column are more widespread but the peak values near region **A** are lower than on April 10. There is clear evidence of transport of ozone perturbations across the Pacific with values of the order of 8 DU appearing near the international dateline and 20°N – 30°N latitude range. The peak changes in BC and OC optical depths (Figure 9 (middle and right)) in the high latitude occur at locations outside the fire zones **B** and **C** due to transport effects, and these changes are larger than on April 10 near regions **B** and **C**. As mentioned before, the MODIS fire count data for the region **C** peaked around April 17. Evidence for transport of the aerosols into the Arctic region is also seen. *Warneke et al.* [2009] suggest that the earlier than usual onset of fire season in 2008 might have enhanced the efficiency of transport of BB emissions into the Arctic region.

[23] The impact of the Asian fires on tropospheric composition averaged over the entire month of April is shown in

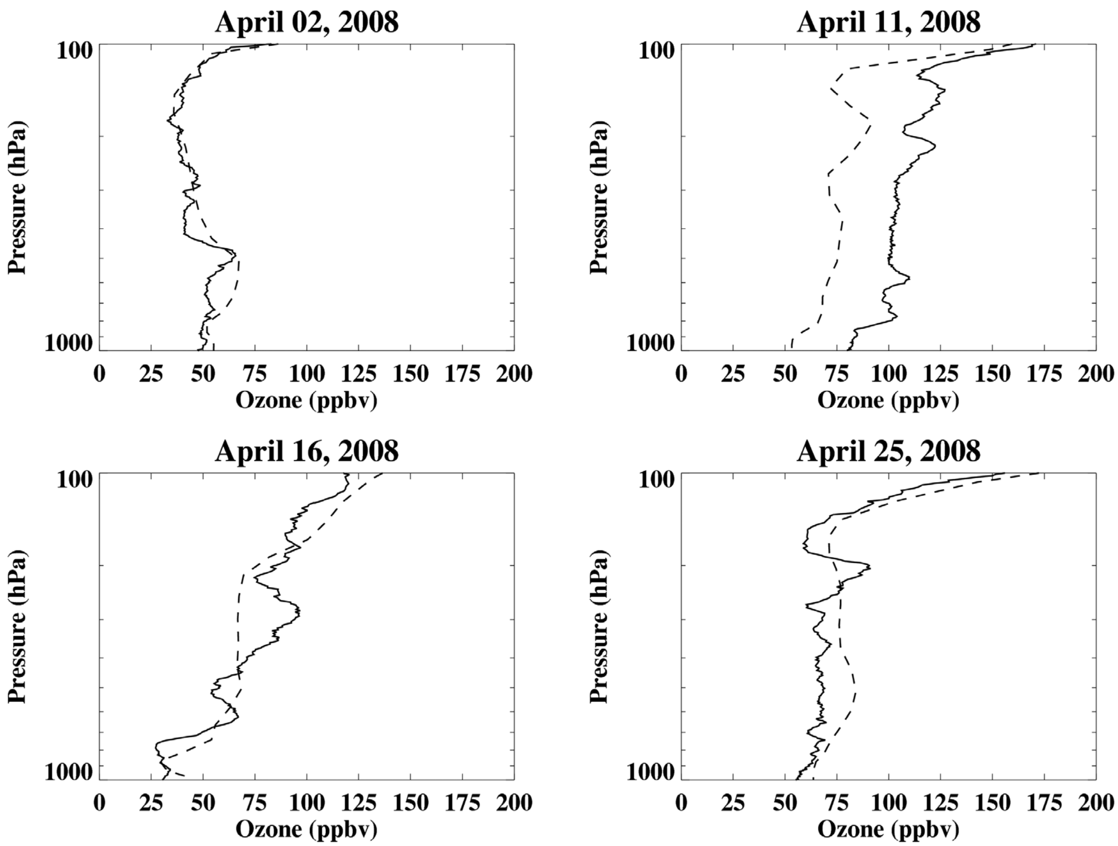

Figure 7. Ozone mixing ratio (ppbv) profiles at Naha (127.7°E, 26.2°N) from Ozonesonde (solid) and RAQMS (dashed). (top left) April 2, 2008; (top right) April 11, 2008; (bottom left) April 16, 2008; (bottom right) April 25, 2008.

Figure 10. Ozone changes are predominant in the low latitude, near the Thailand fire region, with a peak value of the order of 10 DU. Much smaller increases in the tropospheric ozone column are seen nearly throughout the northern hemisphere. The BC and OC AOD changes are also widespread but the peak values are smaller than for a selected day shown earlier. From the results of the baseline and perturbed model runs, we find that, in the longitude sector from 90°E to 135°E and averaged over April 2008, BB emissions from the regions **A**, **B**, and **C** result in an increase in the relative contribution of BC and OC to the total AOD, from about 25% to 80% at 20°N, and from about 40% to 80% at 52°N. The contributions of the Asian fires to the AOD in the tropics and in the region 35°N to 45°N are smaller. The monthly averaged distributions provide a better perspective of the impact of the fires on a regional scale.

3. Radiative Transfer

3.1. Model Description

[24] The objective of this study is to evaluate the radiative impact of the Asian fires, and we do this with the help of an off-line radiative transfer code. The model we use is a recent version of the NASA Langley Fu-Liou code. This is a highly modified version [*Charlock et al.*, 2006; *Rose et al.*, 2006; Kato *et al.*, 2011] of the original model developed by *Fu and Liou* [1993]. The shortwave calculation in this model considers 18 spectral bands and uses a 2-stream procedure; the absorbing gases are H_2O, CO_2, O_3, O_2, and CH_4. The longwave computation uses a combination of 2 and 4-stream approach. H_2O, CO_2, O_3, CH_4, N_2O, and CFCs are the active species in the thermal infrared. The model uses correlated k distributions based on HITRAN 2000 in the shortwave computation. The *Clough et al.* [1989] continuum is used in the longwave. The model assumes an external mixture of gases, clouds and aerosols. Aerosol effects include scattering (SW and LW), absorption (SW and LW), and emission (LW). The aerosol optical properties are adopted from *Hess et al.* [1998]. Properties of water-soluble aerosols are used for OC and those of soot are used for BC. While we have used AERONET and satellite observations for comparisons with the model results, we have not attempted to modify the aerosol optical properties with the help of the data. More information about the radiation code and validations can be seen at the Website of CERES/ARM Validation Experiment (CAVE) http://www-cave.larc.nasa.gov/cave/

[25] Input data for the present calculations include daily averaged pressure, temperature, humidity, and ozone profiles from the RAQMS simulations. The RAQMS simulations include the effects of clouds and aerosols on the photochemistry. In the following discussions of the radiative forcing, the terms 'clear', and 'total sky' conditions refer to the radiative calculations only, and the same ozone profile is used for both cases. Also included are the daily averaged optical depth profiles for different types of aerosols from RAQMS. Daily averaged cloud fraction, liquid water and ice

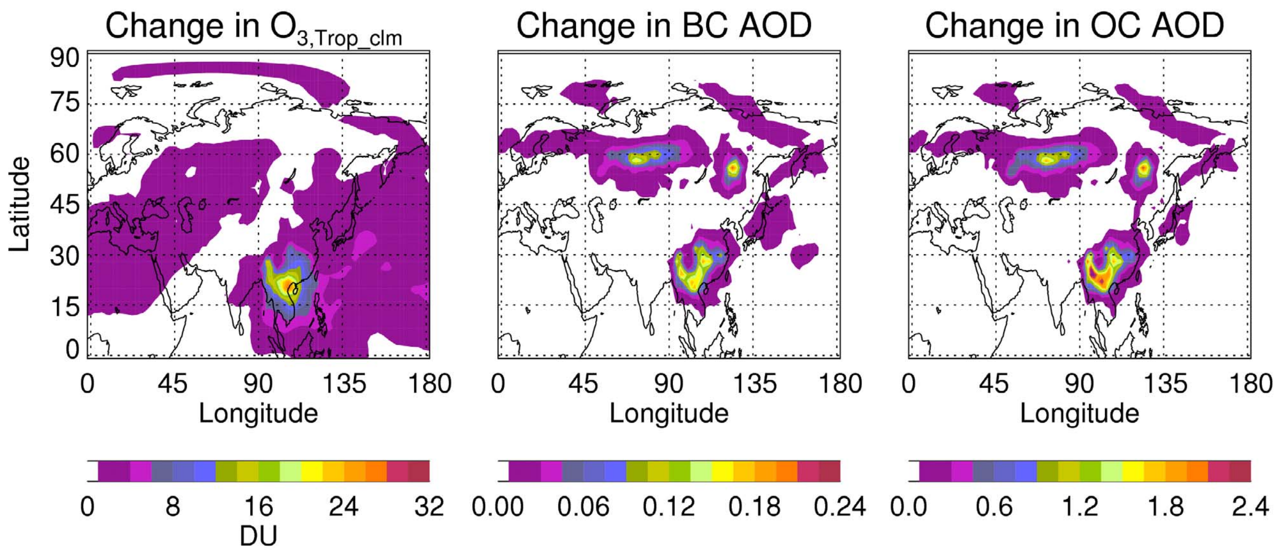

Figure 8. Calculated change, defined as (Baseline-Perturbed), in the tropospheric composition caused by the Asian fires, for April 10, 2008. (left) Change in tropospheric ozone column, DU; (middle) Change in AOD due to BC; (right) Change in AOD due to OC.

concentration profile are taken from the dynamical core (UW-Hybrid) model. Direct and diffuse surface albedo for appropriate solar zenith angles are also obtained from the dynamical model. Shortwave and longwave flux profiles at each grid point of the RAQMS model are evaluated for each day of April 2008. These fluxes are instantaneous fluxes; adjustments due to perturbations in atmospheric temperature are not considered. A Gaussian quadrature is used to get the diurnally averaged shortwave fluxes after repeating the flux calculations at the corresponding solar zenith angles. Net fluxes at the top of the atmosphere (TOA) and at the surface (SRF) are calculated for each day and grid point, for both the baseline and perturbed simulations. The difference between the net fluxes for the baseline (with fires) and the perturbed (without the fires) simulation represents the radiative forcing due to the Asian fire emissions over Thailand (**A**), Kazakhstan (**B**) and Siberia (**C**). It should be noted that we consider only the direct effect of the aerosols, and the shortwave effects due to absorption and scattering predominate. Cloud properties and surface albedo used in the model are not affected by the changes in aerosol amount.

3.2. Radiative Forcing Results

[26] The calculated impact of the Asian fires on the net radiative flux at TOA and SRF is discussed in this section. Just as we did earlier for the changes in composition, we will first describe the radiative effects for two separate days and then discuss the monthly averaged results. These are

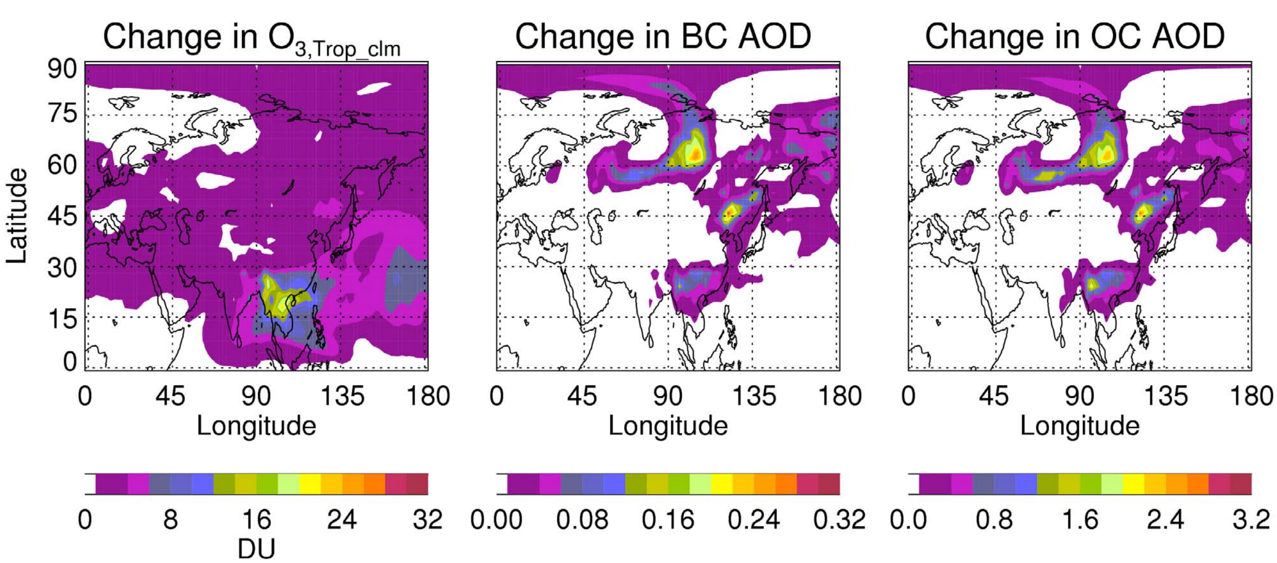

Figure 9. Same as Figure 8, but for April 22, 2008.

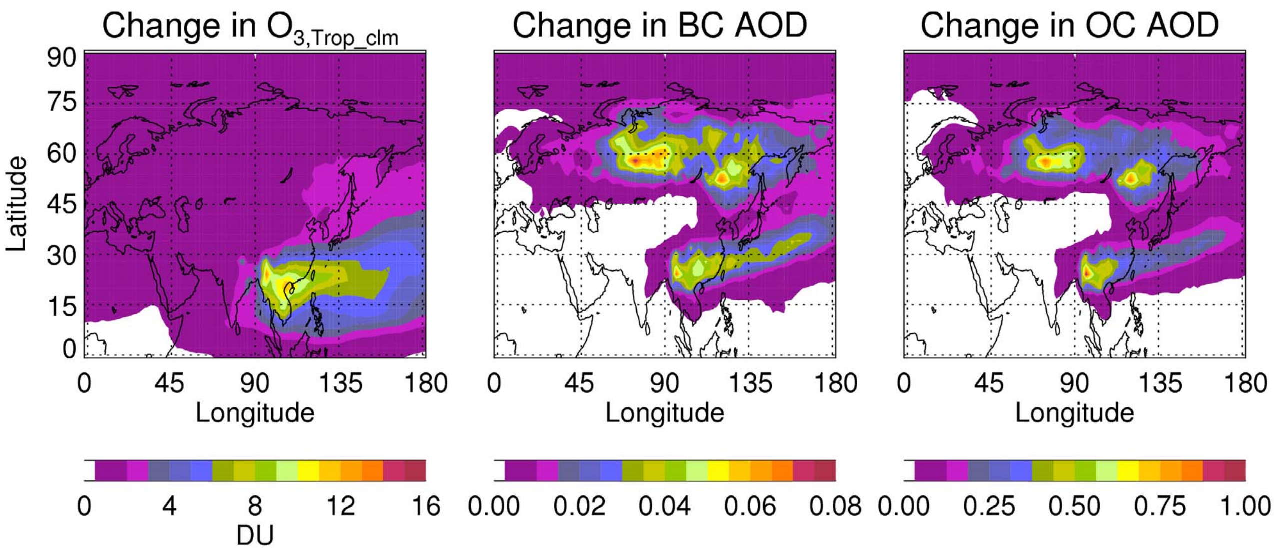

Figure 10. Same as Figure 8, but averaged over the entire month of April, 2008.

combined radiative forcing due to changes in tropospheric ozone and carbonaceous aerosols. We will discuss the forcing due to changes in ozone alone later in the section. Figure 11 shows the radiative impact for April 10 at TOA. Figure 11 (top left) corresponds to the results for clear sky conditions. Large negative forcing, lower than -20 W/m^2, is seen near all the fire regions. This is mainly due to increased upward shortwave flux caused by aerosol scattering. The scattering effects of carbonaceous aerosols clearly dominate over the absorbing effects of BC for clear sky conditions. There is a hint of positive forcing in the Arctic region with peak values at about 74°N and 135°E. The presence of absorbing BC aerosols above a reflecting surface (with high surface albedo) like sea ice could result in such a warming effect [*Haywood and Boucher*, 2000]. Small increases in tropospheric ozone could also provide non-negligible positive forcing. The warming effect is more clearly seen in Figure 11 (right), which shows the radiative impact at TOA for total sky conditions. In this case, large negative forcing is still present close to the fire location. Near region **A**, there is a sizable area with positive forcing which is the result of enhancement of absorbing BC aerosols over the reflective cloud surface. The BC aerosols absorb the reflected shortwave radiation and warm the lower atmosphere. This reduction in the reflected shortwave at TOA shows up as a positive forcing. *Hsu et al.* [2003] report a similar effect in their study of the modulating influence of smoke aerosols on the reflected radiation from clouds. They find that, in Southeast Asia during March 2000, the presence of smoke aerosols over cloudy regions reduces the outgoing shortwave flux at TOA by as much as 100 W/m^2. Their conclusions were based on their analysis of narrowband radiances from Sea viewing Wide Field of view Sensor (SeaWiFS) and Total Ozone Mapping spectrometer (TOMS) and broadband data from Clouds and Earth's Radiant Energy System (CERES) measurements taken in Southeast Asia during March 2000. In Figure 11, areas of positive forcing are also seen in the northern high latitudes of Asia, indicating the effects of the

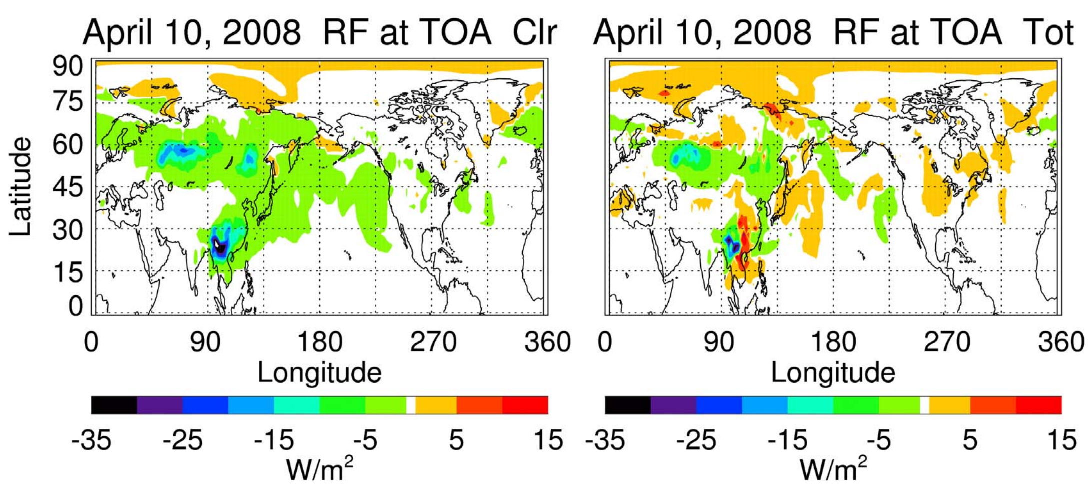

Figure 11. Calculated distribution of radiative forcing due to changes in tropospheric ozone, BC and OC, in W/m^2, for April 10, 2008. (left) At TOA for clear sky; (right) at TOA for total sky.

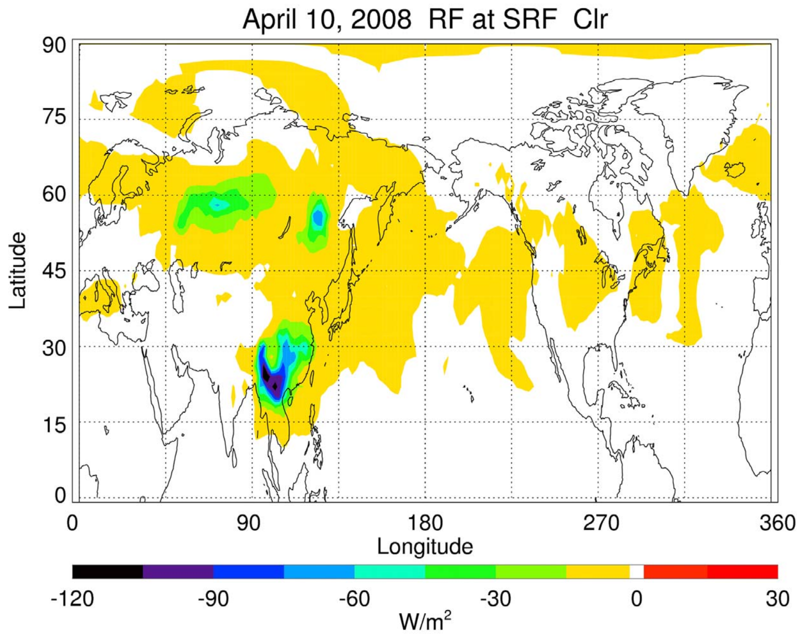

Figure 12. Same as Figure 11, but at the surface and for clear sky.

BC aerosols from the Kazakhstan and Siberian fires. We recognize that the magnitude of radiative forcing due to BC aerosols could be influenced by our assumption of an external mixing state for the aerosols. *Jacobson* [2001] reports that the mixing state of BC approaches that of an internal mixture and that this could result in a higher positive forcing. The radiative forcing at the surface for the clear sky case is shown in Figure 12. Here, both scattering and absorbing effects of the aerosols reduce the shortwave flux arriving at the surface and thus lead to a negative forcing at the surface. The minimum value in the Thailand fire region is -120 W/m^2. For the total sky case (not shown), the calculated impact at the surface is less negative with a minimum value of -111 W/m^2. It should be noted that the cloud properties, such as fractional cloud cover, remain the same for both the baseline and perturbed model simulations. Since the masking effect of the cloud is dominant, perturbation to the net flux at the surface occurs over smaller area corresponding to cloud-free regions and hence the surface radiative forcing due to BB emissions is smaller.

[27] Figure 13 shows the calculated radiative impact of the fires for April 22. At TOA for clear sky conditions (Figure 13, left) large negative forcing is present very near the fire locations indicating the dominance of the aerosol scattering effects. Positive radiative forcing larger than 10 W/m^2 is clearly seen in the Arctic region. The transport of absorbing BC aerosols to a region with high surface albedo due to sea ice is the major reason for the positive forcing. The influence of absorbing BC aerosols is further enhanced by the presence of clouds underneath as seen by the larger areas of positive forcing for the total sky case shown in Figure 13 (right). Such warming influence over an extended period of time could have implications for the fragile Arctic climate. The deposition of the BC aerosols on snow or sea ice surface

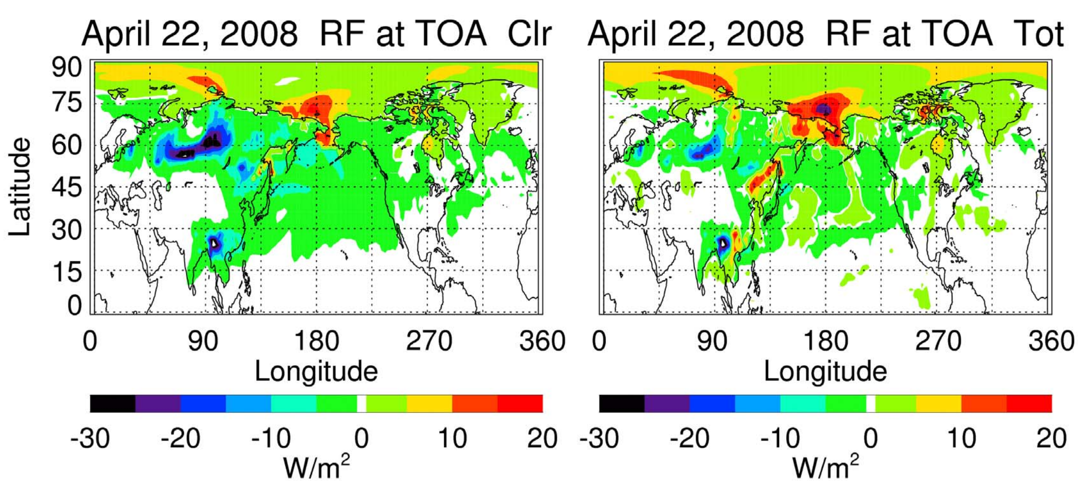

Figure 13. Same as Figure 11, but for April 22, 2008.

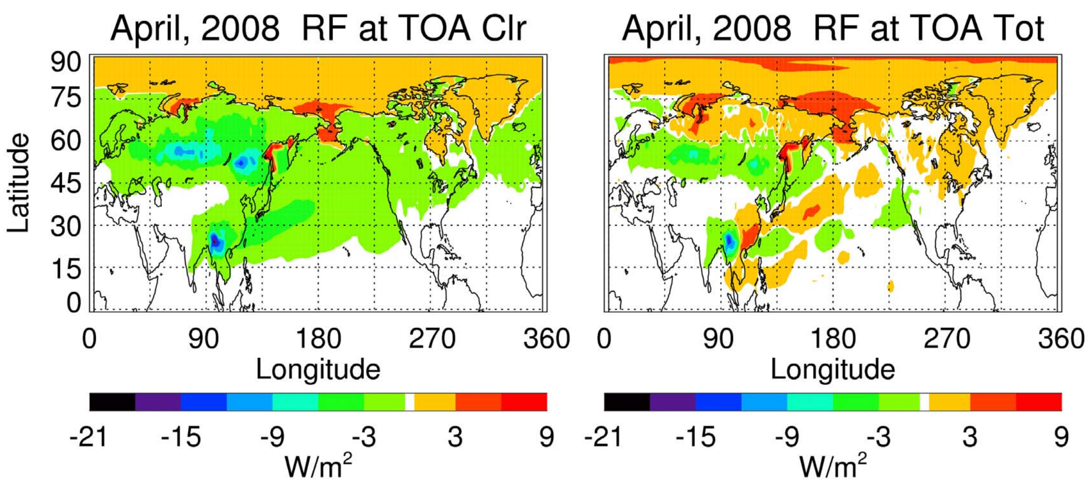

Figure 14. Same as Figure 11, but averaged over the entire month of April, 2008.

could cause a decrease in the surface albedo characteristics and result in a positive radiative forcing [*Hansen and Nazarenko*, 2004]. The present study does not consider indirect effects such as anthropogenic changes in the surface albedo and the attendant radiative forcing. Areas with positive forcing are seen for total sky conditions near the Thailand (**A**) and Siberian (**C**) fires also, highlighting the combined effect of clouds and BC aerosols. The radiative forcing at the surface for April 22, not shown, is similar to that for April 10. For this day, the increase in aerosol-enhanced regions, shown in Figure 9, translates into widespread regions of cooling at the surface.

[28] The monthly averaged radiative forcing due to the emissions from the Asian fires is shown in Figure 14. As in the case of changes in composition, the absolute peak values of the radiative forcing averaged over the month are much lower than for individual days. The peak negative forcing at TOA for clear sky case, (left) is about -20 W/m^2 in the region **A**. Small positive forcing (3 W/m^2 warming) is seen in the Arctic region. More regions of positive forcing are seen for the total sky case shown in Figure 14 (right). The change from the clear sky case is quite significant in the regions affected by the Thailand fire. While the larger values of positive forcing represent the effect of absorbing aerosols, a contribution from increases in the tropospheric ozone to the positive forcing, though small, is present especially at the lower latitudes. As expected, the monthly averaged forcing at the surface for clear sky conditions, shown in Figure 15, is negative in all the regions affected by the fire plumes. It should be recognized that the widespread negative forcing at the surface over extended period of time could alter the surface energy budget. Cooling of the surface, combined with a warming of the atmosphere in the presence of absorbing aerosols, could result in a modification of the stability of the atmosphere. *Liepert et al.* [2004] report that the reduction in evaporation triggered by increases in anthropogenic aerosols over time could lead to a spinning down of the water cycle. The present study does not consider the indirect effects such as the influence of increases in aerosols on the hydrological cycle and on the cloud properties.

[29] In the above discussion of the radiative impact, we have highlighted mainly the role of scattering and absorbing aerosols. They certainly play a major role especially in the high latitude regions. The monthly averaged changes in the composition, shown in Figure 10, indicate that larger changes in ozone occur in the low latitudes near region **A**. Even though we have used the changes in tropospheric ozone column to demonstrate the impact of the Asian fire emissions on ozone, we should point out that the radiative forcing is influenced by the vertical profile of the ozone changes. The radiative flux calculations that we have discussed do incorporate the effect of changes in ozone profiles. It is certainly of interest to look at the relative impact of changes in ozone alone. The radiative transfer model has an option to calculate the fluxes for a pristine atmosphere without any aerosol loading. Using this option, we have calculated the radiative forcing due only to changes in ozone. Since we are interested in the impact of changes in tropospheric ozone, it is better to look at net radiative fluxes at the tropopause level. TOA net flux will be modulated by stratospheric ozone and so it doesn't show the full impact of tropospheric changes. Figure 16 shows the radiative forcing for clear sky conditions at the model tropopause. It should be noted that the color scales for the two panels are different because of the large differences in the ranges of values. Figure 16 (left) shows the monthly averaged combined forcing of changes in carbonaceous AOD and ozone. This is similar to the case shown in Figure 14 except that the forcing is at the tropopause level. The forcing is mostly negative, again reflecting the dominance of the scattering effects of the aerosols under clear sky conditions. Positive forcing in the high latitude and in the Arctic region is caused by the presence of absorbing aerosols over a region of high surface albedo. Figure 16 (right) shows the monthly averaged forcing due to changes in ozone alone. Larger positive forcing is seen in the low latitude affected by the fire in region **A** (Thailand). The maximum forcing near Laos is about 0.5 W/m^2. We get similar results for total sky conditions (not shown). In the case of OC and BC aerosol enhancements, the flux changes are mostly in the shortwave. For O_3 enhancements, shortwave effects are present but are minor compared to the longwave (greenhouse) effect. The reduction in upward longwave flux, both at TOA and at the tropopause, shows up as positive forcing.

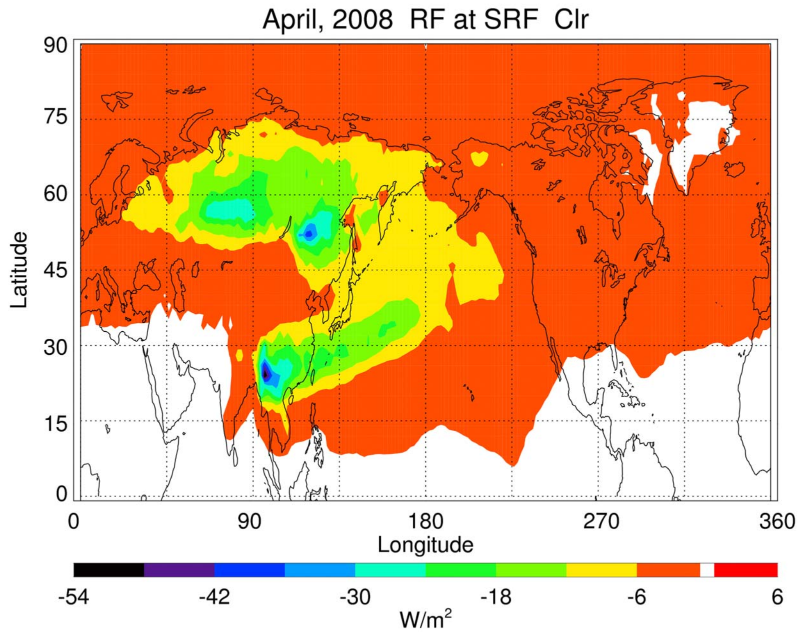

Figure 15. Same as Figure 12, but averaged over the entire month of April, 2008.

[30] We mentioned earlier that because of the short lifetimes of tropospheric ozone and carbonaceous aerosols, the impact on climate due to BB emissions would be more significant on a regional scale than global scale. While the distributions shown earlier highlight the peak values and areal extent of the impact, they do not convey quantitative information for any region or for the globe. We have chosen the region **A** (Thailand and neighboring countries) to evaluate the regional impact of the fire. The selected domain extends from 80°E to 120°E longitude, and from 10°N to 30°N latitude. The monthly averaged radiative impact for this region is shown in Table 2. The two major columns, titled (O_3 + AOD) and (O_3), represent the effects of changes in ozone and carbonaceous AOD and those due to changes in ozone alone respectively. The results from a model sensitivity study, shown in parenthesis, will be discussed later. The radiative forcing for clear sky is -2.546 W/m^2 at TOA and -9.2 W/m^2 at the surface when both ozone and aerosol changes are considered. This results in a net warming of the atmosphere. For total sky, the results are -0.54 W/m^2 and -7.711 W/m^2 at TOA and SRF respectively. Net warming of the atmosphere for total sky case is about 7.17 W/m^2 compared to about 6.65 W/m^2 for the clear sky. This difference is mainly due to the presence of absorbing aerosols above the reflective cloud cover. The radiative forcing due to changes in tropospheric ozone alone is 0.121 W/m^2 at TOA and 0.145 W/m^2 at the surface. The forcing at the tropopause level is 0.249 W/m^2 for clear sky and this is larger than the TOA forcing. The forcing due to ozone alone at the tropopause for total sky

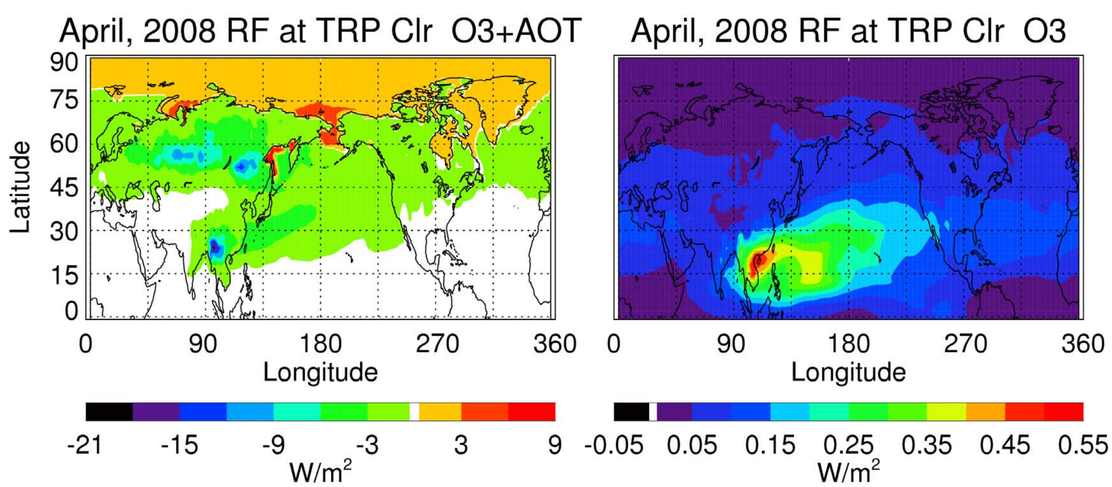

Figure 16. Calculated distribution of radiative forcing at the model tropopause, averaged over the entire month of April, 2008, (left) due to changes in ozone, BC, and OC, and (right) due to changes in ozone alone (Note the different color scales).

Table 2. April 2008 Mean Radiative Forcing (W/m^2) Due to Asian Fire Emissions, Averaged Over the Region From 80°E to 120°E, and From 10°N to 30°N[a]

	O_3 + AOD		O_3	
	Clear	Total	Clear	Total
TOA	−2.546 (−2.066,−2.849)	−0.540 (0.089,−0.917)	0.121	0.120
Tropopause	−2.473 (−1.979,−2.786)	−0.457 (0.189,−0.846)	0.249	0.218
SRF	−9.204 (−10.08,−8.662)	−7.711 (−8.507,−7.204)	0.145	0.077

[a]The two numbers in parenthesis represent the radiative forcing when the single scattering albedos for BC and OC aerosols are modified. The first number corresponds to DRF for SSA-0.03 and the second number corresponds to DRF for SSA + 0.03.

conditions is similar in magnitude (but opposite in sign) to the forcing due to OC+BC and ozone. However, the warming of the troposphere by enhancements in BC aerosols caused by Thailand fires is more significant than that due to increase in ozone alone.

[31] The clear sky forcing at TOA and the surface from this study can be compared with the results reported by *Wang et al.* [2007] on the radiative impact of BB in Southeast Asia.

[32] They used a tracer trajectory model to evaluate the distribution of OC and BC aerosols during March 2001, and a shortwave radiative transfer model to get the DRF of OC, BC and OC+BC aerosols. The clear sky radiative forcing for the region 70°E to 110°E and 5°N to 30°N, in their study, ranged from −1.9 to 0.4 W/m^2 at TOA, and from −0.5 to −12 W/m^2 at the surface. Also, they used a linear fit of the RF to the AOD of aerosols generated by BB to evaluate the radiative forcing efficiency of BC, OC, and BC+OC emitted by BB. For the Southeast Asian region considered in their study, they find the radiative forcing efficiency at TOA for OC+BC, defined as the radiative forcing per unit AOD and represented by the slope of the linear fit, to be −15.0 W/m^2 over land and −28.9 W/m^2 over sea. Similar analysis of the RF in region **A** as a function of the change in AOD of BC+OC in the present study yields a forcing efficiency at TOA of −11.9 W/m^2 for April 2008. This efficiency could be slightly more negative since, in our calculation, the net fluxes include the impact of increases in tropospheric ozone also. At the surface, our value for the radiative forcing efficiency is about −47 W/m^2 compared to their value of −89.4 W/m^2 over land and −93.3 W/m^2 over sea. We cannot derive the forcing efficiency of OC or BC separately from our model results. *Wang et al.* [2007] note that AOD of BC has a dominating influence on the surface forcing efficiency. It is possible that the differences in the OC/BC AOD ratio between the two studies could be the reason for the difference in the forcing efficiency at the surface.

[33] The impact of boreal fire emissions on the arctic atmosphere was one of the major themes of the ARCTAS campaign in 2008. The monthly average radiative forcing shown in Figure 14 indicates noticeable effect in the high latitudes based on our model study. In order to get a quantitative estimate, we have done the regional analysis for the entire hemisphere north of 60°N and the results are listed in Table 3. At the TOA, the forcing for clear sky case is about −0.3 W/m^2, but for total sky there is a change of sign and the calculated forcing of 1.125 W/m^2 represents a warming effect. The surface forcing for both clear and total sky conditions is negative but the magnitude is not as large as in the region **A**, and the surface forcing is less negative for the total sky condition. The warming of the troposphere by about 4 W/m^2 is a significant impact on the arctic climate. The radiative forcing due to changes in tropospheric ozone alone for this high latitude region is much smaller, about 0.04 W/m^2, compared to the region **A**. This is as expected given the smaller perturbations in tropospheric ozone in high latitudes.

[34] Uncertainties in the optical properties, especially those of aerosols, could have a large impact on the calculated radiative forcing. A major parameter of interest in this regard is the single scattering albedo (SSA) of the aerosols, though other properties such as the extinction coefficient and the asymmetry parameter could also be important. *Loeb and Su* [2010] have studied the effects of perturbing the optical parameters of the aerosols on the direct radiative forcing calculated using a radiative transfer model similar to the one used in this study. The combined uncertainty, reported in their study, in the aerosol DRF due to modifications in all the aerosol properties is about 0.5 to 1.0 W/m^2. We have conducted a less elaborate sensitivity analysis by using modifications in only the SSA, and that too only for the OC and BC aerosols. According to *Loeb and Su* [2010], uncertainties in SSA dominate the total combined uncertainty in the aerosol DRF.

[35] Following their procedure, we perturbed the SSA of OC and BC in each grid box and for each of the SW bands by ±0.03. The monthly averaged results with the perturbed SSA are shown within parenthesis in Tables 2 and 3. The two numbers within the parenthesis represent the calculated radiative forcing for a perturbation to SSA of −0.03 and +0.03 respectively. On a regional scale, the range in the radiative forcing at TOA for these perturbations is about 0.6

Table 3. Same as Table 2 Except That the Averaging is Done Over the Entire Hemisphere for Latitudes > 60°N

	O_3 + AOD		O_3	
	Clear	Total	Clear	Total
TOA	−0.301 (0.116, −0.487)	1.125 (1.591, 0.921)	0.026	0.028
Tropopause	−0.426 (−0.019, 0.603)	1.017 (1.474, 0.821)	0.043	0.042
SRF	−4.428 (−4.777, −4.282)	−3.167 (−3.466, −3.038)	0.022	0.009

to 1.0 W/m^2. The impact on the radiative forcing is slightly larger for a negative perturbation in the SSA, thus indicating a higher sensitivity to the presence of absorbing aerosols. The influence of SSA on the calculated radiative forcing is significant and this emphasizes the need for accurate input data. We acknowledge that, besides the optical properties, other factors such as uncertainties in the source gas emissions from fires could also affect the calculated change in the composition and the radiative forcing. Full analysis of these uncertainties is beyond the scope of this study.

4. Summary

[36] We have used a global scale air quality model and an off-line radiative transfer model to study the impact of emissions from Asian fires on the composition and regional scale radiative forcing. This study considers the major fires that occurred in Thailand (**A**), Kazakhstan (**B**), and Siberia (**C**), regions during spring 2008. The main components of the emissions that are of significance to atmospheric radiative transfer are the carbonaceous aerosols (both OC and BC), and precursors for the formation of ozone. We made use of the MODIS rapid analysis data on fire counts along with meteorology-based estimates of fire severity to develop day and night values of BB emission rates for the time period of interest. Our baseline case includes emissions from all the fires, and the perturbed simulation contains no emissions from the Asian fires. The difference between the results from the two model simulations indicates the extent of the perturbations in composition caused by the Asian fire emissions. Increases in monthly averaged tropospheric column ozone of more than 10 DU occur in the low latitude region near the Thailand (**A**) fire zone. Availability of ozone precursors from other anthropogenic sources, combined with the faster photochemistry, in this low latitude region probably enhanced the formation of ozone. The ozone changes in the high latitude regions are not very significant, perhaps indicating the impact of slower photochemistry in the high latitudes during spring. Large increases in OC and BC optical depths are noticed near all the three fire zones. The day-to-day variations in BB emissions and in transport processes result in dramatic changes in the OC and BC distributions throughout the month. As shown in Figure 9, by the 22nd of April, the aerosol perturbations have spread out to the Arctic region. The impact of the boreal fire emissions on the Arctic atmosphere was the focus of the ARCTAS and ARCPAC campaigns in 2008. But a large effect during the spring phase of the campaign was rather unexpected. Calculated AOD distributions are in good agreement with the observations; however, discrepancies do exist in the magnitude of AOD and extinction in some regions. Uncertainties in the emission source strengths and the optical properties of the aerosol used in the model could be partly responsible for these differences.

[37] We use daily averages of the calculated distributions of ozone, OC, and BC, along with the other meteorological parameters from the RAQMS model as input data in an off-line radiative transfer model for evaluating the shortwave and longwave radiative flux distributions. The net flux values at the TOA, tropopause, and the surface from the baseline and perturbed model simulations are used to evaluate the radiative forcing due to fire induced changes. Averaged over the entire month, the increase in the atmospheric reflectivity caused by the additional aerosol loading leads to a 20 W/m^2 negative radiative forcing at the TOA near the fire zones under clear sky conditions. Away from the fire zones, and especially under cloudy conditions, positive radiative forcing is seen. This is mostly due to the transit of absorbing aerosol layer above the highly reflective cloud surface, which warms the atmosphere by absorbing the reflected SW. It is worth noting that, averaged over the month, a warming effect of about 3 W/m^2 is seen in the Arctic region far away from the fire regions, thus highlighting the importance of transport effects and the potential impact on the fragile Arctic climate. At the surface, for both clear and total sky conditions, the predominant radiative forcing is negative. This is mainly due to the increased scattering and absorption of shortwave flux by the OC and BC aerosols. The negative forcing at the surface combined with the warming of the atmosphere in the presence of absorbing aerosols could impact the atmospheric stability and surface energy budget, and spin down the hydrological cycle. Given the short lifetimes of both tropospheric ozone and aerosols, radiative effects of the changes in their abundances are likely to be more significant on a regional basis. The monthly and area weighted average of the radiative forcing at TOA over the region from 80°E to 120°E and from 10°N to 30°N, and for clear sky conditions is -2.546 W/m^2, and the forcing at the surface is -9.2 W/m^2. The atmospheric radiative forcing over the region **A** is about 6.65 W/m^2. This forcing includes the effect of changes in the tropospheric ozone within the selected region. The contribution of changes in ozone alone, averaged over the month and over the region, is 0.145 W/m^2 at TOA and 0.245 W/m^2 at the tropopause. The radiative forcing results shown in this study are critically dependent on the input data and various parameterizations used in the model. This study focused mainly on the direct radiative effect of the OC and BC aerosols and tropospheric ozone generated by the Asian fires. The cloud parameters used in the baseline and perturbed cases are the same and are provided by the UW-Hybrid model, the dynamical core of RAQMS. Therefore, the influence of the clouds in modulating the aerosol effects is considered while the influence of the aerosols on the cloud properties is not. The calculated forcing also depends on the properties of the aerosols used in the model, and on the mixing state of the aerosols. Sensitivity studies conducted with small perturbations of ± 0.03 to the SSA of BC and OC aerosols indicate that the uncertainty in the DRF at TOA could be about 0.6 to 1.0 W/m^2. The sensitivity of DRF to small perturbations in SSA is not significant at the surface and for low latitude, clear sky case at TOA. We note that for high surface reflectance conditions, for example high latitude or total sky case, a small change in SSA has the potential to alter the sign of DRF at TOA [*Haywood and Boucher*, 2000]. Uncertainties in the evaluation of the fire emission data and the injection height of the smoke could also affect the calculated DRF. Future advances in model formulations, quality of the input data, and the availability of observations for comparisons will help to improve our understanding of the regional climatic impact of BB emissions, and add credence to the estimated radiative forcing results which may form a critical input for making policy decisions related to climate change.

[38] **Acknowledgments.** The Tropospheric Chemistry Research Program of NASA Earth Sciences Division supported this research. We thank the reviewers for their suggestions and comments.

References

Al-Saadi, J. A., et al. (2008), Intercomparison of near-real-time biomass burning emissions estimate constrained by satellite fire data, *J. Appl. Remote Sens.*, *2*, 021504, doi:10.1117/1.2948785.

Beer, R., T. A. Glavich, and D. M. Rider (2001), Tropospheric emission spectrometer for the Earth Observing System's Aura satellite, *Appl. Opt.*, *40*, 2356–2367, doi:10.1364/AO.40.002356.

Bian, H., and M. J. Prather (2002), Fast-J2 accurate simulation of stratospheric photolysis in global chemical models, *J. Atmos. Chem.*, *41*, 281–296, doi:10.1023/A:1014980619462.

Bond, T. C., and H. Sun (2005), Can reducing black carbon emissions counteract global warming?, *Environ. Sci. Technol.*, *39*, 5921–5926, doi:10.1021/es0480421.

Bond, T. C., et al. (2004), A technology-based global inventory of black and organic carbon emissions from combustion, *J. Geophys. Res.*, *109*, D14203, doi:10.1029/2003JD003697.

Charlock, T. P., F. G. Rose, D. A. Rutan, Z. Jin, and S. Kato (2006), The global surface and atmospheric radiation budget: An assessment of accuracy with 5 years of calculations and observations, paper presented at the 12th Conference on Atmospheric Radiation, Am. Meteorol. Soc., Madison, Wisc., 10–14 July.

Chin, M., et al. (2002), Tropospheric aerosol optical thickness from the GOCART model and comparisons with satellite and Sun photometer measurements, *J. Atmos. Sci.*, *59*, 461–483, doi:10.1175/1520-0469(2002)059< 0461:TAOTFT>2.0.CO;2.

Chin, M., et al. (2009), Light absorption by pollution, dust, and biomass burning aerosols: A global model study and evaluation with AERONET measurements, *Ann. Geophys.*, *27*, 3439–3464, doi:10.5194/angeo-27-3439-2009.

Chou, M. D., and M. J. Suarez (1999), A solar radiation parameterization for atmospheric studies, *NASA Tech. Memo.*, *TM-1999-104606*, vol. 15, 40 pp.

Chung, C. E., V. Ramanathan, D. Kim, and I. A. Podgorny (2005), Global anthropogenic aerosol direct forcing derived from satellite and ground-based observations, *J. Geophys. Res.*, *110*, D24207, doi:10.1029/2005JD006356.

Clough, S. A., F. X. Kneizys, and R. W. Davies (1989), Line shape and the water vapor continuum, *Atmos. Res.*, *23*, 229–241, doi:10.1016/0169-8095(89)90020-3.

Dupont, R., et al. (2012), Attribution and evolution of ozone from Asian wild fires using satellite and aircraft measurements during the ARCTAS campaign, *Atmos. Chem. Phys.*, *12*, 169–188, doi:10.5194/acp-12-169-2012.

Forster, P., et al. (2007), Changes in atmospheric constituents and in radiative forcing, in *Climate Change 2007: The Physical Science Basis. Contribution of Working Group I to the Fourth Assessment Report of the Intergovernmental Panel on Climate Change*, pp. 131–234, Cambridge Univ. Press, Cambridge, U. K.

Fu, Q., and K. N. Liou (1993), Parameterization of the radiative properties of cirrus clouds, *J. Atmos. Sci.*, *50*, 2008–2025, doi:10.1175/1520-0469(1993)050<2008:POTRPO>2.0.CO;2.

Gauss, M., et al. (2006), Radiative forcing since preindustrial times due to ozone change in the troposphere and lower stratosphere, *Atmos. Chem. Phys.*, *6*, 575–599, doi:10.5194/acp-6-575-2006.

Hansen, J., and L. Nazarenko (2004), Soot climate forcing via snow and ice albedos, *Proc. Natl. Acad. Sci. U. S. A.*, *101*, 423–428, doi:10.1073/pnas.2237157100.

Haywood, J., and O. Boucher (2000), Estimates of the direct and indirect radiative forcing due to tropospheric aerosols: A review, *Rev. Geophys.*, *38*, 513–543, doi:10.1029/1999RG000078.

Hess, M., P. Koepke, and I. Schult (1998), Optical properties of aerosols and clouds: The software package OPAC, *Bull. Am. Meteorol. Soc.*, *79*, 831–844, doi:10.1175/1520-0477(1998)079<0831:OPOAAC>2.0.CO;2.

Hobbs, P. V., J. S. Reid, R. A. Kotchenruther, R. J. Ferek, and R. Weiss (1997), Direct radiative forcing by smoke from biomass burning, *Science*, *275*, 1777–1778, doi:10.1126/science.275.5307.1777.

Holben, B. N., et al. (1998), AERONET: A federated instrument network and data archive for aerosol characterization, *Remote Sens. Environ.*, *66*, 1–16, doi:10.1016/S0034-4257(98)00031-5.

Hsu, N. C., J. R. Herman, and S. C. Tsay, (2003), Radiative impacts from biomass burning in the presence of clouds during boreal spring in southeast Asia, *Geophys. Res. Lett.*, *30*(5), 1224, doi:10.1029/2002GL016485.

Jacobson, M. Z. (2001), Strong radiative heating due to mixing state of black carbon in atmospheric aerosols, *Nature*, *409*, 695–697, doi:10.1038/35055518.

Jacobson, M. Z. (2002), Control of fossil-fuel particulate black carbon and organic matter, possibly the most effective method of slowing global warming, *J. Geophys. Res.*, *107*(D19), 4410, doi:10.1029/2001JD001376.

Joiner, J., et al. (2009), Accurate satellite-derived estimates of the tropospheric ozone impact on the global radiation budget, *Atmos. Chem. Phys.*, *9*, 4447–4465, doi:10.5194/acp-9-4447-2009.

Kahn, R. A., et al. (2008), Wildfire smoke injection heights: Two perspectives from space, *Geophys. Res. Lett.*, *35*, L04809, doi:10.1029/2007GL032165.

Kato, S., et al. (2011), Improvements of top-of-atmosphere and surface irradiance computations with CALIPSO-, CloudSat-, and MODIS-derived cloud and aerosol properties, *J. Geophys. Res.*, *116*, D19209, doi:10.1029/2011JD016050.

Keil, A., and J. M. Haywood (2003), Solar radiative forcing by biomass burning aerosol particles during SAFARI 2000: A case study based on measured aerosol and cloud properties, *J. Geophys. Res.*, *108*(D13), 8467, doi:10.1029/2002JD002315.

Liepert, B. G., J. Feichter, U. Lohmann, and E. Roeckner (2004), Can aerosols spin down the water cycle in a warmer and moister world?, *Geophys. Res. Lett.*, *31*, L06207, doi:10.1029/2003GL019060.

Loboda, T. V., and I. A. Csiszar (2007), Reconstruction of fire spread within wildland fire events in northern Eurasia from the MODIS active fire product, *Global Planet. Change*, *56*, 258–273, doi:10.1016/j.gloplacha.2006.07.015.

Loeb, N. G., and W. Su (2010), Direct aerosol radiative forcing uncertainty based on a radiative perturbation analysis, *J. Clim.*, *23*, 5288–5293, doi:10.1175/2010JCLI3543.1.

Naik, V., et al. (2005), Net radiative forcing due to changes in regional emissions of tropospheric ozone precursors, *J. Geophys. Res.*, *110*, D24306, doi:10.1029/2005JD005908.

Naik, V., et al. (2007), On the sensitivity of radiative forcing from biomass burning aerosols and ozone to emission location, *Geophys. Res. Lett.*, *34*, L03818, doi:10.1029/2006GL028149.

Olivier, J. G. J., A. F. Bouwman, C. W. M. Vander Maas, J. J. M. Berdowski, C. Veldt, J. P. J. Bloos, A. J. H. Visschedijk, P. Y. J. Zandveld, and J. L. Haverlag (1996), Description of EDGAR Version 2.0: A set of global emission inventories of greenhouse gases and ozone-depleting substances for all anthropogenic and most natural sources on a per country basis and on $1^\circ \times 1^\circ$ grid, *Rep. 771060 002*, 141 pp., RIVM, Bilthoven, Netherlands.

Pierce, R. B., et al. (2003), Regional Air Quality Modeling System (RAQMS) predictions of the tropospheric ozone budget over East Asia, *J. Geophys. Res.*, *108*(D21), 8825, doi:10.1029/2002JD003176.

Pierce, R. B., et al. (2007), Chemical data assimilation estimates of continental U.S. ozone and nitrogen budgets during the Intercontinental Chemical Transport Experiment-North America, *J. Geophys. Res.*, *112*, D12S21, doi:10.1029/2006JD007722.

Ramanathan, V., and G. Carmichael (2008), Global and regional climate changes due to black carbon, *Nat. Geosci.*, *1*, 221–227, doi:10.1038/ngeo156.

Ramanathan, V., P. J. Crutzen, J. T. Kiehl, and D. Rosenfeld (2001), Aerosols, climate, and the hydrological cycle, *Science*, *294*, 2119–2124, doi:10.1126/science.1064034.

Reddy, M. S., O. Boucher, Y. Balkanski, and M. Schulz (2005), Aerosol optical depths and direct radiative perturbations by species and source type, *Geophys. Res. Lett.*, *32*, L12803, doi:10.1029/2004GL021743.

Rose, F., T. P. Charlock, Q. Fu, S. Kato, D. Rutan, and Z. Jin (2006), CERES Proto-Edition 3 radiative transfer: Model tests and radiative closure over surface validation sites, paper presented at the 12th Conference on Atmospheric Radiation, Am. Meteorol. Soc., Madison, Wisc., 10–14 July.

Ross, J. L., and P. V. Hobbs (1998), Radiative characteristics of regional hazes dominated by smoke from biomass burning in Brazil: Closure tests and direct radiative forcing, *J. Geophys. Res.*, *103*(D24), 31,925–31,941, doi:10.1029/97JD03677.

Sander, S. P., et al. (2003), Chemical kinetics and photochemical data for use in atmospheric studies, *Eval. 14*, NASA Jet Propul. Lab., Calif. Inst. of Technol, Pasadena, Calif.

Schaack, T. K., T. H. Zapotocny, A. J. Lenzen, and D. R. Johnson (2004), Global climate simulation with the Univ. of Wisconsin global hybrid isentropic coordinate model, *J. Clim.*, *17*, 2998–3016, doi:10.1175/1520-0442(2004)017<2998:GCSWTU>2.0.CO;2.

Soja, A. J., et al. (2004), AVHRR-derived fire frequency, distribution, and area burned in Siberia, *Int. J. Remote Sens.*, *25*(10), 1939–1960, doi:10.1080/01431160310001609725.

Streets, D. G., et al. (2003), An inventory of gaseous and primary aerosol emissions in Asia in the year 2000, *J. Geophys. Res.*, *108*(D21), 8809, doi:10.1029/2002JD003093.

Verma, S., et al. (2009), Ozone production in boreal fire smoke plumes using observations from the Tropospheric Emission Spectrometer and the Ozone Monitoring Instrument, *J. Geophys. Res.*, *114*, D02303, doi:10.1029/2008JD010108.

Wang, S. H., N. H. Lin, M. D. Chou, and J.-H. Woo (2007), Estimate of radiative forcing of Asian biomass-burning aerosols during the period of TRACE-P, *J. Geophys. Res.*, *112*, D10222, doi:10.1029/2006JD007564.

Warneke, C., et al. (2009), Biomass burning in Siberia and Kazakhstan as an important source for haze over the Alaskan Arctic in April 2008, *Geophys. Res. Lett.*, *36*, L02813, doi:10.1029/2008GL036194.

Warneke, C., et al. (2010), An important contribution to springtime Arctic aerosol from biomass burning in Russia, *Geophys. Res. Lett.*, *37*, L01801, doi:10.1029/2009GL041816.

Winker, D. M., W. H. Hunt, and M. J. Mcgill (2007), Initial performance assessment of CALIOP, *Geophys. Res. Lett.*, *34*, L19803, doi:10.1029/2007GL030135.

Worden, H. M., et al. (2007), Comparisons of Tropospheric Emission Spectrometer (TES) ozone profiles to ozonesondes: Methods and initial results, *J. Geophys. Res.*, *112*, D03309, doi:10.1029/2006JD007258.

Yu, H., et al. (2010), Global view of aerosol vertical distributions from CALIPSO lidar measurements and GOCART simulations: Regional and seasonal variations, *J. Geophys. Res.*, *115*, D00H30, doi:10.1029/2009JD013364.

T. P. Charlock, M. Natarajan, J. A. Al-Saadi, and D. M. Winker, NASA Langley Research Center, Hampton, VA 23681, USA. (murali.natarajan@nasa.gov)

A. J. Lenzen and T. K. Schaack, SSEC, University of Wisconsin, Madison, WI 53706, USA.

R. B. Pierce, NOAA/NESDIS/STAR, Madison, WI 53706, USA.

F. G. Rose, Science Systems and Applications, Inc., Hampton, VA 23666, USA.

A. J. Soja, National Institute of Aerospace, Hampton, VA 23666, USA.

J. R. Worden, Jet Propulsion Laboratory, Pasadena, CA 91109, USA.